Available online at www.sciencedirect.com

SciVerse ScienceDirect

Journal of the European Ceramic Society 32 (2012) 765–776

www.elsevier.com/locate/jeurceramsoc

Synthesis of diphosphate $Mn_{2-x}Mg_xP_2O_7$ solid solutions with thortveitite structure: New pink ceramic dyes for the colouration of ceramic glazes

M. Llusar*, A. García, C. Gargori, R. Galindo, J.A. Badenes, G. Monrós

Departamento de Química Inorgánica y Orgánica, Universitat Jaume I, 12071 Castellón, Spain

Received 13 August 2011; received in revised form 21 October 2011; accepted 29 October 2011
Available online 21 November 2011

Abstract

Solid solutions of Mn and Mg mixed diphosphates $Mn_{2-x}Mg_xP_2O_7$ ($0.2 < x < 1.5$) have been prepared by calcination (1000 °C/4 h) of coprecipitate precursors and characterized for the first time (through thermal analysis, XRD, SEM/EDX and UV–vis-NIR techniques). Its colouring performance (CIE-$L^*a^*b^*$ parameters) within a ceramic glaze has been also analyzed. XRD and SEM/EDX results confirm the formation of a homogeneous and continuous β-$Mn_{2-x}Mg_xP_2O_7$ solid solution having the thortveitite structure, isomorphous to β-$Mn_2P_2O_7$ and β-$Mg_2P_2O_7$. The diphosphates exhibit light brown or pinkish-white colours associated to Mn^{2+} ions in low-symmetry octahedral coordination. Interestingly, they develop intense purple ($x < 1$) or pink ($1.0 \leq x \leq 1.5$) colours once enamelled (5 wt.%) within a single-firing ceramic glaze, which are mainly associated to the presence of Mn^{3+} ions according to UV–vis-NIR spectra. Therefore, the Mn–Mg binary diphosphates could be used as new pink ceramic dyes for the colouration of conventional ceramic glazes.

Keywords: A. Sol–gel processes; C. Colour; C. Optical Properties; Diphosphates; Pink ceramic dyes

1. Introduction

Divalent metal diphosphates or pyrophosphates $M_2P_2O_7$ may present many different polymorphic modifications. The two major classes of polymorphism in metal diphosphates are concerned with the adoption of either the thortveitite ($Sc_2Si_2O_7$) or the dichromate structure types.[1–3] In addition, they may exhibit also different temperature-dependent polymorphic modifications, the low-temperature α form and the higher temperature forms (β, γ, δ, etc.).[1,4,5] Many diphosphates of small divalent cations (such as Mg or a first series transition metal from Cr to Zn) adopt the thortveitite structure as their high temperature β modifications,[6–9] while for larger divalent metals (such as Ca, Sr, Ba, Cd and Pb) the dichromate-type structure is generally observed.[2,3] The crystalline structure of thortveitite-based β-diphosphates (monoclinic *C2/m* space group) is characterized by having a staggered (non-eclipsed) conformation of $P_2O_7^{2-}$ anions, with almost linear P–O–P bonds and an irregular octahedral coordination for the divalent cations. During cooling all these thortveitite-based β-diphosphates, with the exception of $Mn_2P_2O_7$, experience reversible solid state phase transitions to the low-temperature modifications (α forms). In comparison to the isomorphous β series, the structures of α-diphosphates exhibit bent P–O–P angles, with the cations lying in both sixfold and fivefold coordination, and may crystallize in different monoclinic space groups of lower symmetry such as *B21/c* or *P21/c* (M = Mg, Co or Ni), *C2/c* (M = Cu) or *I2/c* (M = Zn).[8,9] Noteworthy, in the case of mixed metal or binary diphosphates, $M_{2-x}A_xP_2O_7$ (with M or A being also Mg or a 3d transition metal), the formed solid solutions may present at room temperature the structure of the thortveitite β-modification, without transition to the α-form (as in $Mn_2P_2O_7$), or also the low-temperature α-form, depending on the involved metals (this is referenced and discussed with more details in Section 3.2).

In the last decades, many research works have been conducted concerning mixed metal binary diphosphates, which may present improved properties as compared with single metal diphosphates.[10] The studies on these mixed metal diphosphates have been focused on crystallochemical aspects as well as on their many different properties or widespread applications (catalytic, dielectric, ferroelectric, optic, magnetic, environmental,

* Corresponding author at: Departament de Química Inorgànica y Orgànica, Universitat Jaume I, Edifici Científico-Tècnic, Av. Sos Baynat s/n, 12071 Castelló, Spain. Tel.: +34 964 728244; fax: +34 964 728214.
E-mail address: mllusar@qio.uji.es (M. Llusar).

0955-2219/$ – see front matter © 2011 Elsevier Ltd. All rights reserved.
doi:10.1016/j.jeurceramsoc.2011.10.051

etc.).[10–17] More recently, several studies have also analyzed the possible application of some mixed metal orthophosphates and condensed phosphates (pyrophosphates, cyclotetraphosphates, etc.) as inorganic pigments. Onoda et al., for instance, have reported about the synthesis and characterization of inorganic pigments based on different mixed metal phosphates containing transition metals (Co, Ni, Mn and Cu) and also rare earths (La, Nd, Ce, etc.).[18–20] Through the doping with rare earth elements the acid–base resistance of the mixed phosphates was improved, which is of paramount importance for their application as inorganic pigments. However, in all these studies their performance as ceramic pigments or dyes for the colouration of ceramic glazes was not investigated. In contrast with a ceramic dye, a ceramic pigment is generally insoluble and exhibits a low affinity or reactivity with the substrate or medium to which is added (ceramic glaze, porcelainized stoneware, etc.) during the firing treatment.

Concerning this issue, in previous works we reported about the characterization and possible application of different Co–Fe mixed phosphates or oxy-phosphates as ceramic pigments or dyes,[21,22] and the colouring performance within a conventional ceramic glaze of mixed metal $(Mn,Mg)Fe_4(PO_4)_6$ orthophosphates was also investigated.[23] Regarding to condensed pyrophosphates, the solid solutions of Co and Mg mixed diphosphates $Co_{2-x}Mg_xP_2O_7$ were also recently characterized as alternative blue-violet ceramic pigments.[24] In this system, a continuous and homogeneous solid solution formed within the whole experimental range ($0.1 < x < 1.8$), crystallizing with the structure of the low-temperature α-modification, isomorphous to single metal α-$Co_2P_2O_7$ and α-$Mg_2P_2O_7$ diphosphates (*B21/c* symmetry, standardized to *P21/c* space group). The doping with Mg ion is not only justified for its lower economical cost and less harmful environmental or toxic effects, but also for the high chemical and thermal stability of magnesium phosphates.[25] Moreover, in our investigations we have noticed that Mg addition enables also to reduce or eliminate the occurrence of enamelling defects in the fired glaze, such as the well-known "pin-hole" effect.

Following with these investigations, in the present study we report on the synthesis and characterization of Mn and Mg mixed diphosphates $Mn_{2-x}Mg_xP_2O_7$ through diverse techniques (thermal analysis, XRD, SEM/EDX and UV–vis-NIR). In previous studies of Maass about $M_{2-x}Mg_xP_2O_7$ mixed diphosphates (M = Cr–Cu),[13,26] the formed Mn–Mg diphosphates crystallized with the thortveitite (β) structure (isostructural to β-$Mg_2P_2O_7$ and $Mn_2P_2O_7$).[26] However, only two compositions ($x = 0.8$ and 1.0) were studied and, as far as we are concerned, further investigations on these binary Mn–Mg diphosphates are practically absent in the literature. Herein we analyze for the first time the possibility to form a continuous and homogeneous $Mn_{2-x}Mg_xP_2O_7$ solid solution series having the thortveitite structure within a more extended compositional range ($0.2 < x < 1.5$). Given the high thermal and chemical stability of Mg and Mn phosphates, and also considering the light pink colours associated to Mn phosphates, we have tested as well the potential use of the prepared Mn–Mg binary diphosphates as alternative pink ceramic pigments or dyes, analyzing their stability and colouring performance within a conventional single-firing ceramic glaze.

Table 1
Nomenclature of the theoretical (initial) formulations $Mn_{2-x}Mg_xP_2O_7$ prepared by the coprecipitation route.

Sample	Theoretical formulation
M1 ($x = 0$)	$Mn_2P_2O_7$
M2 ($x = 0.2$)	$Mn_{1.8}Mg_{0.2}P_2O_7$
M3 ($x = 0.5$)	$Mn_{1.5}Mg_{0.5}P_2O_7$
M4 ($x = 0.7$)	$Mn_{1.3}Mg_{0.7}P_2O_7$
M5 ($x = 1.0$)	$MnMgP_2O_7$
M6 ($x = 1.2$)	$Mn_{0.8}Mg_{1.2}P_2O_7$
M7 ($x = 1.5$)	$Mn_{0.5}Mg_{1.5}P_2O_7$

2. Materials and methods

2.1. Sample preparation

A solid solution series of Mn and Mg binary diphosphates with compositions $Mn_{2-x}Mg_xP_2O_7$ ($x = 0$, 0.2, 0.5, 0.7, 1.0, 1.2 and 1.5) was prepared through the conventional coprecipitation route, using $Mn(NO_3)_2{\cdot}4H_2O$ (97%, Aldrich), $Mg(NO_3)_2{\cdot}6H_2O$ (99%, Aldrich) and H_3PO_4 (80%, Fluka) as precursors. Table 1 indicates the nomenclature used for the prepared formulations. In a typical preparation, Mg and Mn salts were added (in this order) to an aqueous solution (150 mL) containing the required stoichiometric amount of H_3PO_4 (continuously stirred and at room temperature). Aqueous ammonia (NH_3:H_2O = 1:1) was then added dropwise to the homogeneous solution until reaching a pH of *ca.* 7–7.5. The obtained coprecipitate powders were then dried overnight in an electrical dryer (at 110 °C), and the resulting dried powders were subsequently submitted to calcination in an electrical furnace up to 1000 °C (5 °C/min of heating gradient and 4 h of soaking time at the maximum temperature).

2.2. Sample characterization

Simultaneous differential thermal and thermo-gravimetric analysis (DTA-TGA) of dried coprecipitates was carried out with a Mettler Toledo thermal analyzer (using Pt crucibles with a constant 10 °C/min heating from 25 °C up to 1200 °C). Crystallochemical characterization of calcined samples was performed by X-ray diffraction (XRD) in a Siemens D-500 powder Diffractometer with CuK_α radiation (from 15° to 60° 2θ, with steps of 0.02° 2θ and a counting time of 10 s per step). The diffractometer was equipped with a graphite secondary monochromator to eliminate the K_β and fluorescence signals (important in compositions with a large amount of Mn). Moreover, the cell parameters of 1000 °C-fired diphosphates were also calculated with the *TOPAS* program[27,28] using refined XRD patterns.

On the other hand, the morphology and microstructure of $Mn_{2-x}Mg_xP_2O_7$ solid solution samples obtained after calcination was examined by scanning electron microscopy (SEM) with a Leo-440i Leica electron microscope (following conventional preparation and imaging techniques). The composition and chemical homogeneity of the samples (Mn:Mg:P

molar ratio) was determined by semi-quantitative elemental analysis with an EDX analyzer (supplied by Oxford University) attached to the microscope.

In order to analyze the stability and optical or colouring properties of the obtained solid solutions within a conventional ceramic glaze, the 1000 °C-fired powders were also 5 wt.% enamelled within a commercial single-firing transparent glaze (SiO_2–Al_2O_3–CaO–ZnO system) onto conventional ceramic biscuits, and fired following a fast-firing scheme (52 min of duration from cool to cool at a maximum temperature of 1080 °C). The optical properties of fired powders and enamelled samples were then analyzed by diffuse reflectance spectroscopy (UV–vis-NIR) performed with a Jasco V670 spectrophotometer. The colour parameters ($L^*a^*b^*$) were also measured following the CIE-$L^*a^*b^*$ colourimetric method recommended by the CIE (Commission Internationale de l'Eclairage),[29] using a 8/d (diffused illumination of 8°) geometry, with the observer at 10° and a standard lighting D65 (in agreement with ASTM E 308-85 standard). On this method, L^* is the lightness axis (black (0) → white (100)), b^* is the blue (−) → yellow (+) axis, and a^* is the green (−) → red (+) axis.

Finally, the dispersion and possible interaction or solubilization of the diphosphate particles within the glassy matrix during enamel firing were investigated through SEM observations and EDX analyses, performed onto the surface of enamelled samples. To complement this analysis, the particle size distribution of the fired powders was previously measured with a Mastersizer 2000 (Malvern) laser diffraction equipment (see Supplementary data in Appendix A). This information is relevant, since a different particle size of the fired powders could result in a different chemical resistance during enamel firing, affecting also to their colouring performance (colour saturation, shade, etc.).

3. Results and discussion

3.1. Thermal analysis (DTA-TGA)

The differential thermal (DTA) and thermogravimetric (TGA) analyses of the precursor mixtures (coprecipitates) showed in all cases similar curves, with only minor differences arising from the replacement of Mn by Mg in the compositions. In Fig. 1 we show the thermal analyses of two compositions selected as representatives, a sample with a low Mg content (M2, with $x = 0.2$) and another Mg-enriched (M7, with $x = 1.5$). XRD characterization of raw samples (not shown for brevity reasons) showed that all coprecipitate powders consisted of a mixture of monohydrated ammonium metallophosphates ($NH_4MPO_4 \cdot H_2O$, with M = Mn, Mg) and ammonium nitrate and, accordingly, the obtained DTA-TG curves of raw powders must be consistent with de decomposition processes of these ammono compounds. In this respect, it has been reported that ammonium manganese phosphate monohydrate ($NH_4MnPO_4 \cdot H_2O$) decompose in two or three main steps[30]: the first two steps (between 150 °C and 320 °C) are partially overlapped and correspond to the endothermic deammination and dehydration processes ($NH_4MnPO_4 \cdot H_2O(s) \rightarrow MnHPO_4(s) + NH_3(g) + H_2O(g)$), with an important associated weight loss (around 19%). Then, the

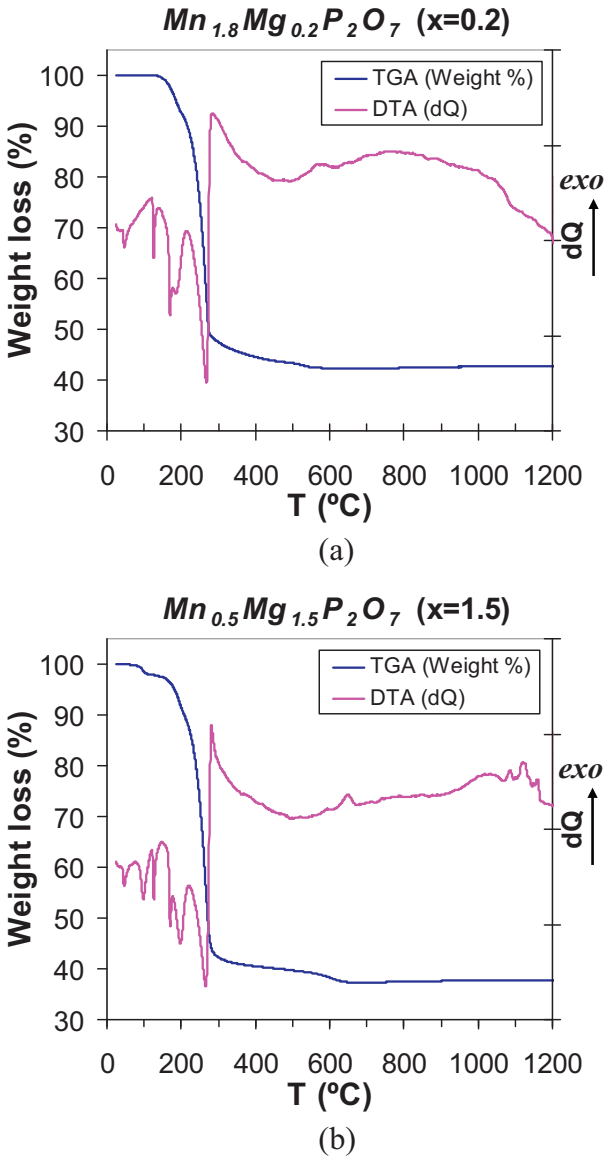

Fig. 1. DTA-TG curves of selected $Mn_{2-x}Mg_xP_2O_7$ samples: (a) $x = 0.2$ and (b) $x = 1.5$.

third step (between 320 °C and 550 °C) corresponds to the polycondensation or dimmerization reaction (with intramolecular dehydration) leading to the formation of manganese pyrophosphate ($MnHPO_4 \rightarrow 1/2Mn_2P_2O_7 + 1/2H_2O$), which is accompanied by a gradual and less pronounced weight loss (around 5–6%). In the case of $NH_4MgPO_4 \cdot H_2O$ (dittmarite), a similar decomposition pattern occurs, with the elimination of water and ammonia molecules (between 190 °C and 325 °C) being followed by a gradual weight loss (325–650 °C) due to the dimmerization of the hydrogenphosphate group and formation of Mg diphosphate ($Mg_2P_2O_7$).[31] In some cases, a partial dehydration has been also observed at lower temperatures (80–187 °C).[32] On the other hand, ammonium nitrate (NH_4NO_3) melts at around 170 °C and then decomposes exothermically around 200–290 °C into water and nitrous oxide ($NH_4NO_3(m) \rightarrow 2H_2O(g) + N_2O(g)$).

The shown DTA-TG curves (Fig. 1) of selected samples (M2 and M7) are in accordance with these processes, and only reflect slight differences due to the increased Mg content. In sample M2 ($x = 0.2$), for instance, after the removal of adsorbed water (*ca.* 0.3 wt.%) below 140 °C, with two associated endothermic peaks at 51 and 127 °C, a partially overlapped two-step weight loss is observed between 140–200 °C (around 7.5%) and 200–310 °C (*ca.* 46%), corresponding to the elimination of water and ammonia molecules of $NH_4(Mn,Mg)PO_4{\cdot}H_2O$ and also owing to NH_4NO_3 decomposition. The first two processes are accompanied by endothermic peaks at 190 and 269 °C, while the additional sharp endothermic peak observed at 170 °C could be assigned to the melting of ammonium nitrate. The decomposition of this compound would be responsible of the exothermic effect with a maximum around 290 °C, and its associated weight-loss would overlap with the last part of the deammination and dehydration processes. Finally, a gradual and softer weight loss (*ca.* 5%) takes place between 320 °C and 600 °C, that could be assigned to the polycondensation or dimmerization reaction leading to the formation of $(Mn,Mg)_2P_2O_7$ diphosphate. Indeed, the small exothermic effect appearing at around 585 °C could be ascribed to the crystallization of this mixed metal diphosphate, in agreement with previous observations.[30]

In the case of sample M7, doped with a much higher amount of Mg ($x = 1.5$), similar features can be observed in the DTA-TG curves. This time, the elimination of adsorbed water (endothermic peaks around 50 and 127 °C) could be overlapped by a partial dehydration at lower temperatures of the ammonium metallophosphate (weight loss around 2%), in agreement with previous observations[32] and being responsible for the additional endothermic peak at 101 °C. Then, the subsequent elimination of ammonia and the remaining hydration water (endothermic peaks at 200 and 269 °C), with an associated weight loss of *ca.* 6.5% (150–200 °C) and *ca.* 49.5% (200–310 °C), would be partially overlapped with the melting (endothermic peak at 170 °C) and decomposition of ammonium nitrate (exothermic peak at 283 °C). Again, the final and gradual weight loss (5%) between 310 and 650 °C would correspond to the polycondensation of the hydrogenphosphate groups and formation of $(Mn,Mg)_2P_2O_7$ diphosphate, the crystallization of which is accompanied by a small exothermic effect at around 656 °C. Thus, the crystallization of the binary diphosphate is slightly shifted to higher temperatures (from 585 °C to 656 °C) as the Mg doping is increased (from $x = 0.2$ to $x = 1.5$).

Also noticeable, in all samples we could not observe below 1200 °C any intense endothermic band associated to the melting of pyrophosphates (i.e. the melting point of $Mg_2P_2O_7$ is 1395 °C). The possible starting of an endothermic band above 1050–1100 °C could only be appreciated in the DTA curves of samples with a lower Mg doping (see for instance in sample M2, with $x = 0.2$). This was not visible in Mg-enriched samples, in which the presence of some small exothermic effects around 1100 °C (see for instance in sample M7, with $x = 1.5$) could be presumably due to the incongruent melting of the formed binary diphosphates. Anyway, these results confirm that all the prepared diphosphates are thermally stable at least below 1100 °C.

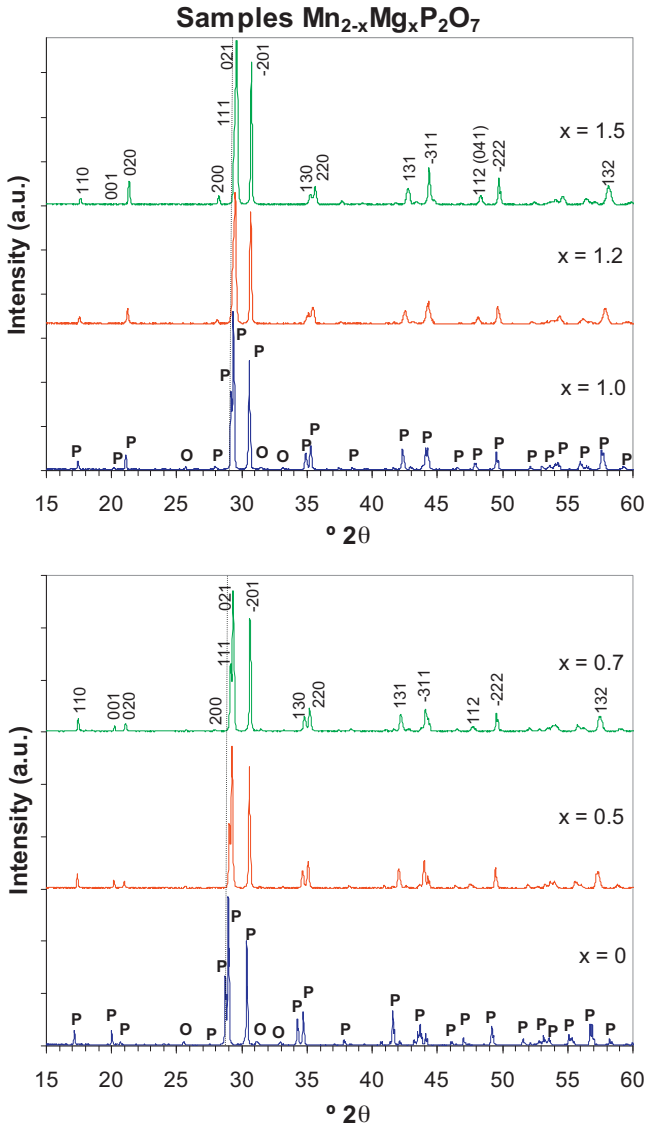

Fig. 2. XRD patterns of representative $Mn_{2-x}Mg_xP_2O_7$ samples fired at 1000 °C/4 h. Crystalline phases: P = $Mn_{2-x}Mg_xP_2O_7$ solid solution, O = $M_3(PO_4)_2$ (with M = Mn or Mn + Mg).

3.2. X-ray diffraction characterization (XRD)

The XRD patterns of representative $Mn_{2-x}Mg_xP_2O_7$ compositions fired at 1000 °C/4 h are shown in Fig. 2. While $Mn_2P_2O_7$ may only adopt the thortveitite β-structure at room temperature (no phase transition to the low-temperature α-modification has been observed above −60 °C), Mg diphosphate may present both structures, β-$Mg_2P_2O_7$ (monoclinic *C2/m* space group, PDF number 073-0535 and ICSD[33] file 22328) and α-$Mg_2P_2O_7$ (monoclinic *P21/c* spatial group, PDF number 072-0019 and ICSD file 15326), and a reversible transition to the low temperature isotype (β → α) occurs at around 68 °C.[6,8,9] Since $Mn_2P_2O_7$ (monoclinic *C2/m* space group, PDF number 077-1244 and ICSD file 47137) is isostructural to the high temperature β-$Mg_2P_2O_7$ polymorph, it is expected that the prepared mixed metal Mn and Mg diphosphates $Mn_{2-x}Mg_xP_2O_7$ crystallize at room temperature also

Table 2
Calculated cell parameters (using the TOPAS fitting program)[27] for representative $Mn_{2-x}Mg_xP_2O_7$ powders (1000 °C-fired).

Sample	Cell parameters (a, b, c and β) and cell volume (V) of $Mn_{2-x}Mg_xP_2O_7$ solid solution[a]				
	a (Å)	b (Å)	c (Å)	β	V (Å^3)
$Mn_2P_2O_7$ (PDF 77-1244)	6.6330	8.5840	4.5460	102.67	252.54
$x = 0.0$	6.6348 (2)	8.5802 (2)	4.5452 (1)	102.740 (2)	252.38 (1)
$x = 0.2$	6.6220 (1)	8.5521 (2)	4.5421 (1)	102.831 (1)	250.805 (9)
$x = 0.5$	6.6034 (2)	8.5121 (3)	4.5365 (2)	102.997 (2)	248.46 (2)
$x = 0.7$	6.5844 (3)	8.4759 (3)	4.5298 (2)	103.125 (3)	246.20 (2)
$x = 1.0$	6.5584 (2)	8.4219 (3)	4.5190 (2)	103.338 (2)	242.87 (1)
$x = 1.2$	6.5419 (4)	8.3928 (5)	4.5176 (3)	103.478 (4)	241.21 (3)
$x = 1.5$	6.5192 (3)	8.3471 (4)	4.5119 (3)	103.663 (3)	238.57 (2)
β-$Mg_2P_2O_7$ (PDF 73-0535)	6.4940	8.2800	4.5220	103.80	236.13

[a] The standard deviation (of the last figure) is shown between brackets.

with the thortveitite (β) structure, similarly to other binary diphosphates such as β-$Mg_{2-x}Cr_xP_2O_7$,[13] β-$Mg_{2-x}Cu_xP_2O_7$[14] or β-$Mn_{2-x}Ni_xP_2O_7$.[16] Indeed, Maass observed the crystallization of β-$Mn_{2-x}Mg_xP_2O_7$ in the only two compositions analyzed in his study ($x = 0.8$ and 1.0).[26] In contrast, other binary diphosphates have been found to crystallize with the low-temperature α-form (such as α-$Co_{2-x}Mg_xP_2O_7$[11,24] and α-$Ni_{2-x}Mg_xP_2O_7$[12]), since in these systems the single metal α-diphosphates are all isostructural (*P21/c* spatial group).

As it can be observed in Fig. 2, a continuous β-$Mn_{2-x}Mg_xP_2O_7$ solid solution formed successfully within the whole studied experimental range ($0.2 \leq x \leq 1.5$) adopting the thortveitite structure, isotypic to the pure phases $Mn_2P_2O_7$ and β-$Mg_2P_2O_7$. Indeed, as the Mg content (x) increases the position of the peaks shifts gradually to higher 2θ values, in accordance with the unit cell contraction caused by the entrance of the smaller Mg^{2+} ions, and the relative intensities of the peaks also change. For instance, the intensities of the 0 2 0 and 2 0 0 peaks, around 21 and 28° 2θ, become steadily higher as the Mg content increases. Moreover, the successful formation of the β-$Mn_{2-x}Mg_xP_2O_7$ solid solution is further evidenced by the presence of only a very minor or negligible amount of $M_3(PO_4)_2$ orthophosphate as secondary phase (with M = Mn or Mn + Mg) for $x \leq 1.0$, and also by the measured cell parameters. In this respect, Table 2 summarizes the cell parameters and cell volume calculated with the TOPAS program from refined XRD patterns.[27] As it may be also appreciated in Fig. 3, there is a linear tendency in the variation of cell parameters of $Mn_{2-x}Mg_xP_2O_7$ diphosphates with the composition (x). The calculated cell parameters (a, b and c) decrease linearly with increasing amounts of Mg (x) in the formulation. As a result, the overall cell volume of the solid solution also diminishes, being compressed between the standard values indexed for single metal $Mn_2P_2O_7$ and $Mg_2P_2O_7$ diphosphates (PDF files 077-1244 and 073-0535, respectively). This is in accordance with the smaller ionic size of Mg^{2+} in six-fold coordination (86 pm), with respect to the size of 6-coordinated (high spin) Mn^{2+} (97 pm).[34] Remarkably, it must be also highlighted that the b-axis diminishes about 2 and 4 times more than a- and c-axis, respectively, which is indicative of a considerable anisotropy in the unit cell variation.

3.3. Electron microscopy characterization (SEM/EDX)

To gain further information about the morphology, homogeneity and semiquantitative composition of the samples at the microscale, SEM/EDX characterization was performed with selected fired samples. SEM observations of the selected $Mn_{2-x}Mg_xP_2O_7$ powders calcined at 1000 °C are shown in Fig. 4 (samples with $x = 0$, $x = 0.5$, $x = 1.0$ and $x = 1.5$). As it may be appreciated, the morphology is quite homogeneous and similar in all samples, irrespective of the amount of Mg doping. In general terms, all the samples are formed by aggregates of heterogeneous sizes (from 5 to *ca.* 50 μm), as it may be better visualized in the SEM image of sample M1 (Fig. 4a), obtained at a lower magnification (x1000). Moreover, these aggregates are constituted in all samples by smaller and interconnected round-grained particles (*ca.* 1–3 μm), giving rise to large and open macropores (around 1 μm-sized). A similar grained-like morphology was observed in the case of Co and Mg mixed diphosphates ($Co_{2-x}Mg_xP_2O_7$).[24]

On the other hand, to determine the chemical composition and homogeneity of the obtained diphosphate solid solutions, semiquantitative EDX analyses were performed in different regions of the samples. In Fig. 5 we show the EDX spectra collected from the areas shown in the SEM images of Fig. 4. In general terms, the analyses showed that the samples were quite homogeneous, obtaining only a slight dispersion in the molar Mn:Mg:P ratios through the different analyzed regions. The

Table 3
Theoretical (initial) formulations and the corresponding EDX-measured average compositions for selected $Mn_{2-x}Mg_xP_2O_7$ coprecipitate samples (1000 °C-fired powders).

Sample	Theoretical formulation	Average EDX composition (atomic)[a]		
		Mn	Mg	P
$x = 0.0$	$Mn_2P_2O_7$	2.0 (2)	–	2.0 (2)
$x = 0.2$	$Mn_{1.8}Mg_{0.2}P_2O_7$	1.9 (3)	0.19 (1)	2.0 (1)
$x = 0.5$	$Mn_{1.5}Mg_{0.5}P_2O_7$	1.4 (3)	0.5 (1)	2.00 (8)
$x = 0.7$	$Mn_{1.3}Mg_{0.7}P_2O_7$	1.32 (6)	0.65 (6)	2.00 (4)
$x = 1.0$	$Mn_{1.0}Mg_{1.0}P_2O_7$	0.98 (9)	0.93 (8)	2.00 (8)
$x = 1.5$	$Mn_{0.5}Mg_{1.5}P_2O_7$	0.48 (4)	1.47 (7)	2.00 (6)

[a] The compositions have been normalized to 2 mol of P. The standard deviation (of the last figure) is shown between brackets.

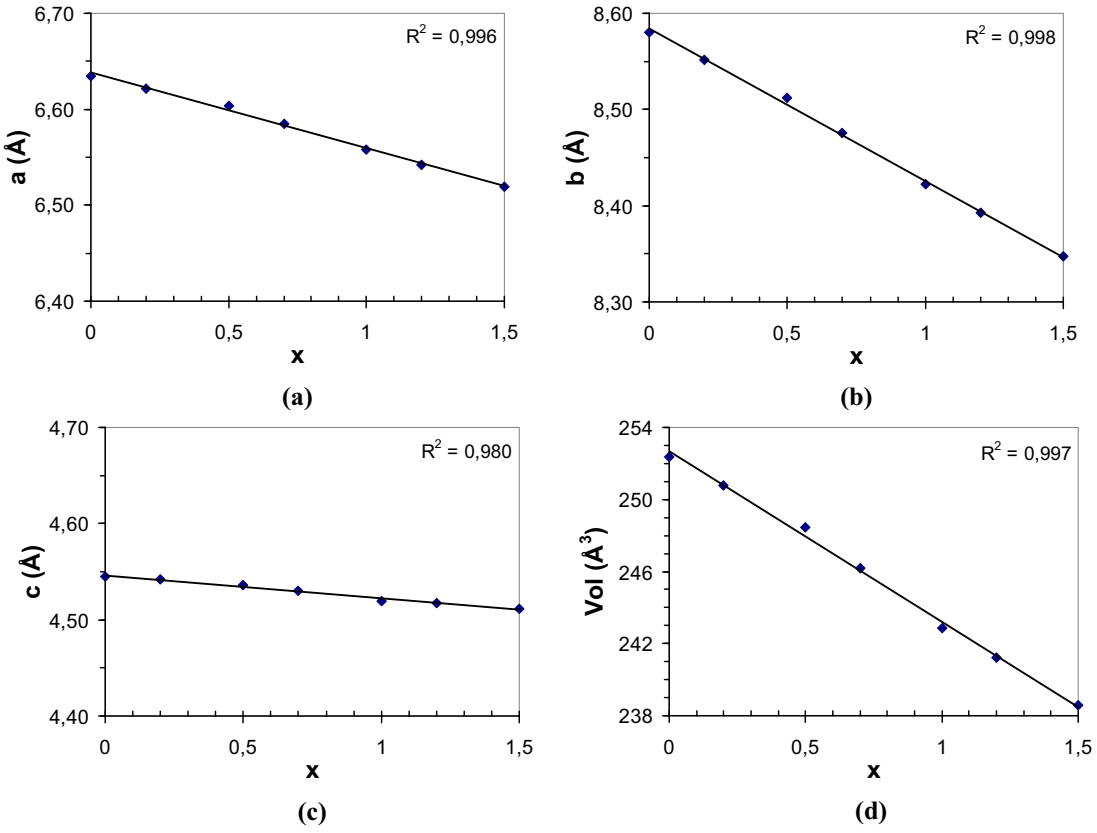

Fig. 3. . Evolution of cell parameters *a*, *b* and *c* (a–c), and cell volume (d) with Mg doping (*x*) for the prepared $Mn_{2-x}Mg_xP_2O_7$ diphosphate solid solutions ($x = 0$, 0.2, 0.5, 0.7, 1.0, 1.2 and 1.5) fired at 1000 °C/4 h (obtained from the TOPAS fitting[27]).

theoretical and experimental (EDX-measured) average compositions of selected samples are summarized in Table 3. As it may be observed the experimental (semiquantitative) compositions are quite close to the theoretical initial formulations.

3.4. UV–vis-NIR spectroscopy and colour characterization

The UV–vis-NIR optical spectra of representative diphosphate $Mn_{2-x}Mg_xP_2O_7$ powders fired at 1000 °C/4 h are shown in Fig. 6 (above). The absorbance spectra of all powdered samples exhibit a broad, weak and multiple band extending from 300 to *ca.* 650 nm, which becomes steadily less intense as the Mg content (*x*) in the formulation is increased, replacing for Mn. The occurrence of these bands of very weak intensity may be unambiguously ascribed to the presence of Mn^{2+} ions in the irregular octahedral sites of the diphosphate thortveitite structure. Indeed, Mn^{2+} ions (d^5) have a ground level $^6A_{1g}(^6S)$ configuration in octahedral (and tetrahedral) coordination and the electronic transitions to the excited states give rise to very weak absorption bands, since they are doubly forbidden (parity forbidden by the Laporte rule and also spin forbidden due to the different multiplicity of the excited states).[35] In agreement with previous studies reporting the electronic spectra of Mn^{2+} phosphates (including $Mn_2P_2O_7$),[36] the obtained optical spectra show the typical bands associated to the crystalline field spin-forbidden transitions of Mn^{2+} ions in low-symmetry octahedral coordination: the prevailing and typical sharp transition ν_3 ($^6A_1(S) \rightarrow {}^4E$, $^4A(G)$) at 404 nm, and the associated and partially overlapped ν_2 ($^6A_1(S) \rightarrow {}^4T_2(G)$) and ν_1 ($^6A_1(S) \rightarrow {}^4T_1(G)$) transitions around 420–460 and 460–600 nm, respectively. In addition, the broad and multiple absorption between 300 and 370 nm could be also assigned to the transitions to the higher energy terms (D and P) of Mn^{2+}: ν_6 ($^6A_1(S) \rightarrow {}^4T_1(P)$) at 314 nm, ν_5 ($^6A_1(S) \rightarrow {}^4E(D)$) at 337 nm, and ν_4 ($^6A_1(S) \rightarrow {}^4T_2(D)$) at 354 nm.[36]

As a result of this broad absorption below 600–620 nm, the obtained 1000 °C-fired diphosphates exhibited light brown ($x < 1$) or pinkish-white ($1.0 \leq x \leq 1.5$) pale colourations. Table 4 shows the measured CIE-$L^*a^*b^*$ colour parameters of the different diphosphate $Mn_{2-x}Mg_xP_2O_7$ powders. As it may be

Table 4
Colour parameters ($L^*a^*b^*$) of $Mn_{2-x}Mg_xP_2O_7$ fired powders (1000 °C) and enamelled samples (single-firing glaze, 1080 °C).

Sample	$L^*/a^*/b^*$ parameters	
	Fired powders	Single-firing glaze
$x = 0$	79.7/3.5/7.5	40.8/7.9/−4.5
$x = 0.2$	81.7/2.7/5.5	37.0/7.9/−3.9
$x = 0.5$	84.0/2.1/4.2	36.5/9.2/−2.4
$x = 0.7$	83.7/1.8/3.9	39.5/10.2/−1.7
$x = 1$	84.4/1.3/3.1	46.0/10.6/0.2
$x = 1.2$	90.5/1.1/−0.7	51.2/10.5/1.1
$x = 1.5$	90.4/0.7/−0.6	60.0/10.4/5.0

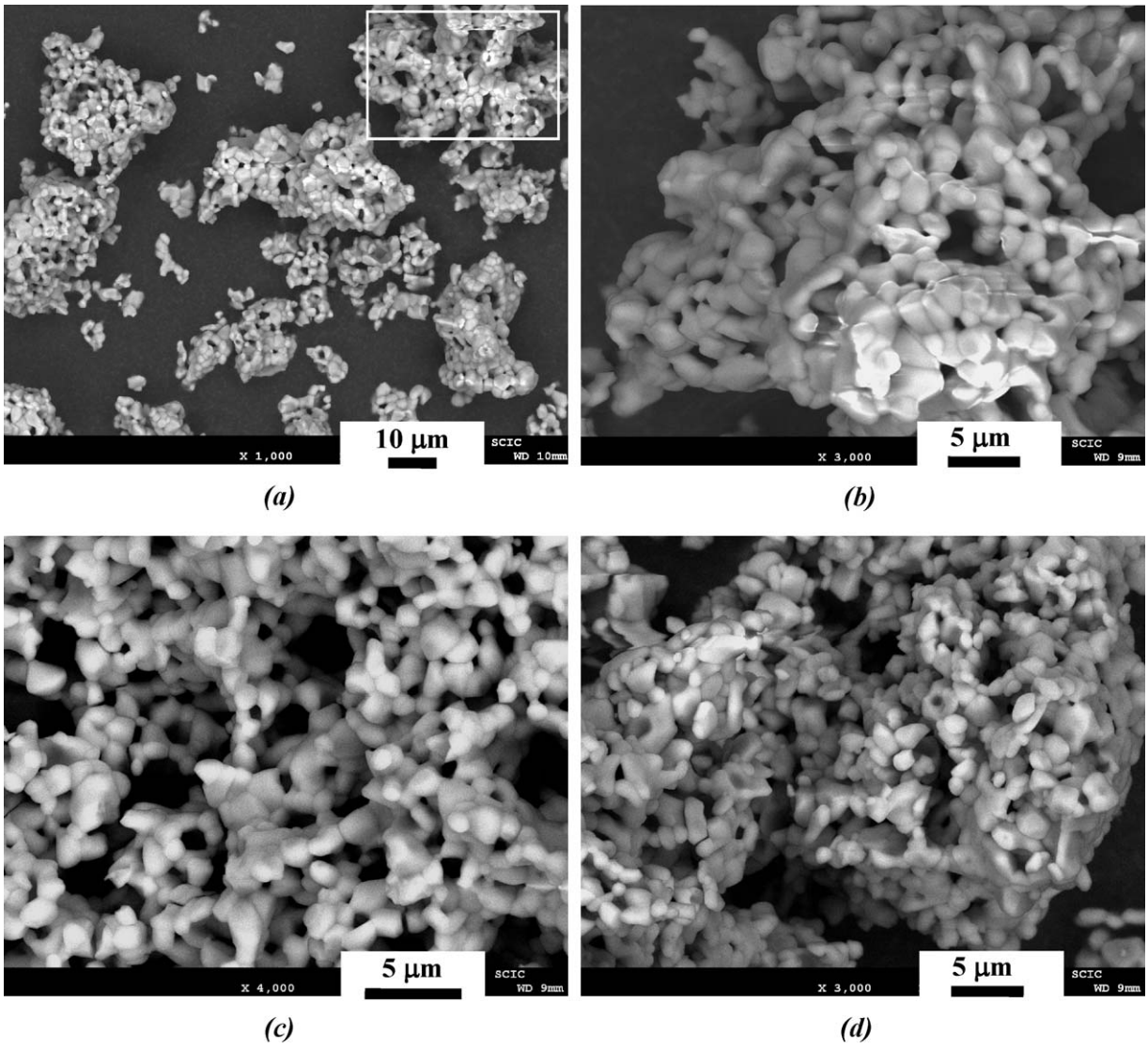

Fig. 4. SEM images (backscattering detector) corresponding to selected 1000 °C-fired samples: (a) M1 ($x = 0$; $Mn_2P_2O_7$), (b) M3 ($x = 0.5$; $Mn_{1.5}Mg_{0.5}P_2O_7$), (c) M5 ($x = 1.0$; $Mn_{1.0}Mg_{1.0}P_2O_7$) and (d) M7 ($x = 1.5$; $Mn_{0.5}Mg_{1.5}P_2O_7$).

appreciated, the powders become slightly redder (higher positive a^* values) and yellowier (higher positive b^* values) the higher the Mn content (lower x value), which results in light or pale brown colours for $x < 1$. In contrast, the Mg-enriched diphosphates ($1.0 \leq x \leq 1.5$) posses very high L^* values (84.4–90.5) and small a^* and b^* values, indicative of pale pinkish (or pinkish white) colours.

Given the light brown or pinkish colours exhibited by the prepared diphosphate solid solutions, in the last part of our investigation we tested also their stability and colouring performance within a conventional ceramic glaze. It is well known that manganese phosphate compounds may give rise to nice pink or purple colourations in glassy systems, the developed colour depending on the Mn content and relative abundance of Mn^{2+} and Mn^{3+} ions.[37] Accordingly, the thortveitite-based $Mn_{2-x}Mg_xP_2O_7$ diphosphates could find technological application as new pink or purple ceramic dyes. For this study we selected a glaze composition (SiO_2–Al_2O_3–CaO–ZnO system) typical of a single-firing schedule (enamel firing at 1080 °C), which is more frequently used in the ceramic tile industry. Interestingly, the enamelled samples developed intense purple ($x < 1$) or pink ($1.0 \leq x \leq 1.5$) colours once enamelled (5 wt.%) within the single-firing ceramic glaze. The visual aspect of enamelled samples may be appreciated in Fig. 7.

Noteworthy, the absorbance spectra corresponding to enamelled samples (Fig. 6, below) presented clearly distinct features than those observed in diphosphate powders (Fig. 6, above). Distinctly, the spectra of enamelled samples showed a strong and broad absorption band extending from 400 to 800 nm. This strong-intensity band cannot be associated to Mn^{2+} ions, since these species usually originate low-intensity (doubly forbidden) bands below *ca.* 600 nm, with a typical sharp peak around 404 nm (ν_3 transition) as the most characteristic feature (as it was previously observed with diphosphate powders). In agreement with previous studies on Mn-containing glasses, the observed complex band may be mainly ascribed to the

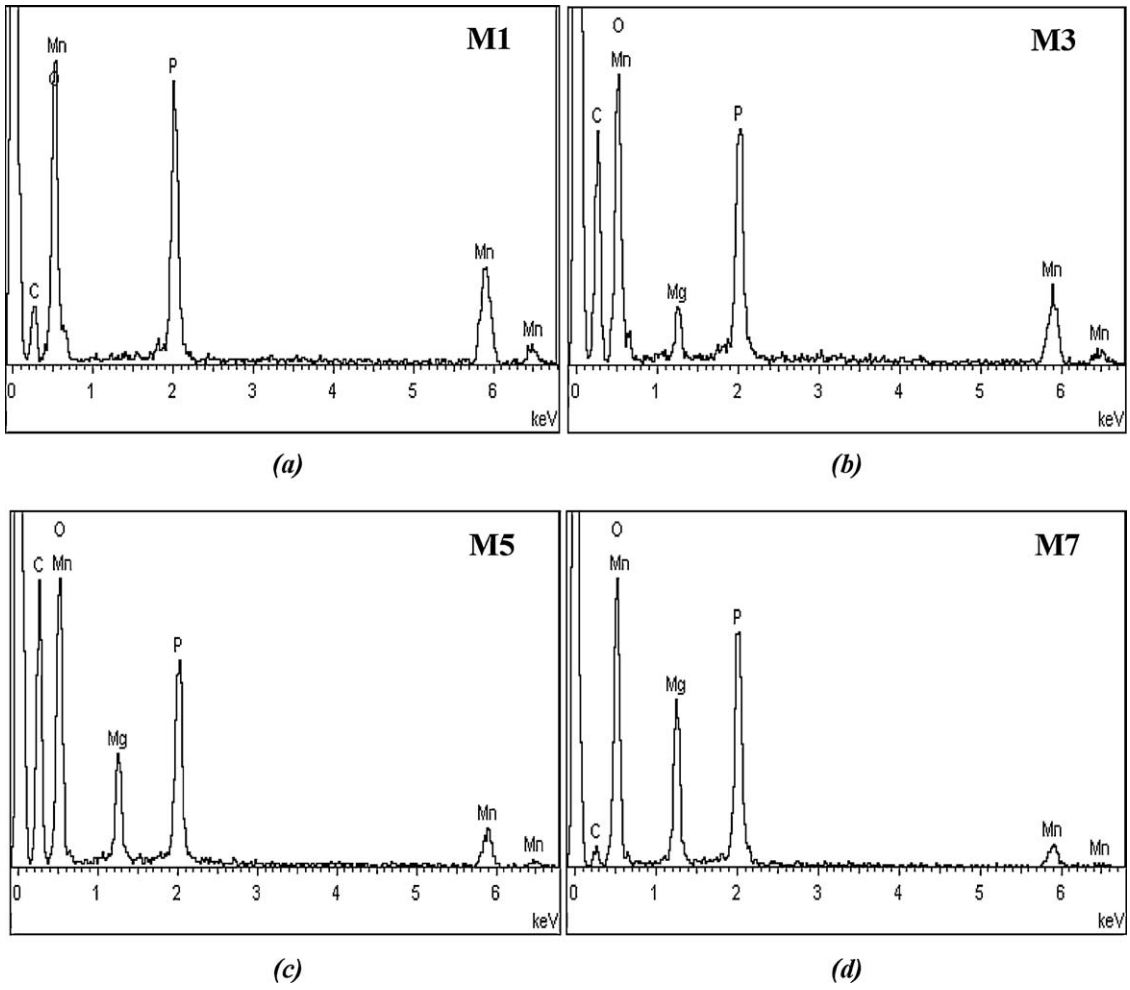

Fig. 5. EDX spectra of selected 1000 °C-fired samples (corresponding to the regions shown in the SEM images in Fig. 4: the area included in the rectangle for sample M1, and the whole area for the other samples): (a) M1 ($x = 0$; $Mn_2P_2O_7$), (b) M3 ($x = 0.5$; $Mn_{1.5}Mg_{0.5}P_2O_7$), (c) M5 ($x = 1.0$; $Mn_{1.0}Mg_{1.0}P_2O_7$) and (d) M7 ($x = 1.5$; $Mn_{0.5}Mg_{1.5}P_2O_7$).

presence of octahedrally coordinated Mn^{3+} ions (d^4 configuration), which exhibit a characteristic broad and multiple band around 400–800 nm, usually centred at 510–530 nm, and which is associated to the spin-allowed, three-fold split transition $^5E_g(^5D) \rightarrow {}^5T_{2g}(^5D)$.[37–40] In addition, the obtained optical spectra also showed an important absorption below 400 nm, as a result of the intense charge transfer (CT) excitations from oxygen to manganese ions.[37] Thus, the observed spectra of enamelled samples indicate that a considerable amount of Mn^{2+} ions was oxidized to Mn^{3+} in the ceramic glaze during enamel firing. This oxidation from Mn^{2+} to Mn^{3+} is also commonly found when melting manganese-containing phosphate glasses, and a melt reduction process must be employed to maintain manganese in the Mn^{2+} oxidation state.[37] In any case, the presence of some amount of Mn^{2+} ions in enamelled samples should not be completely discarded, since the broad and intense band associated to Mn^{3+} ions would be masking the less intense absorption bands of Mn^{2+} ions appearing below 600–620 nm. Anyway, the optical spectra of $Mn_{2-x}Mg_xP_2O_7$ enamelled samples are clearly dominated by the more intense Mn^{3+} absorption features, and the observed complex band has a stronger intensity (the maximum centred at around 500 nm) as the amount of Mn is increased in the formulation (lower x).

As a result of the broad absorption around 500 nm, the enamelled samples with a lower Mg doping ($x < 1.0$) developed very intense purple colours (see Fig. 7), while the colour became pink for lower Mn contents ($1.0 \leq x \leq 1.5$). The corresponding $L^*a^*b^*$ colour parameters of enamelled samples are also shown in Table 4. As it may be appreciated, the L^* values (brightness index) diminish slightly from $x = 0$ (40.8) to $x = 0.5$ (36.5), and then become gradually higher (36.5 → 60.0) as the Mg doping increases ($x > 0.5$), indicative of less dark or less intense colours. On the other hand, samples with $x < 1$ present positive a^* values (red hue) and negative b^* values (blue hue), in correlation with the observed purple colours, while samples M5, M6 and M7 ($1.0 \leq x \leq 1.5$) exhibit nice and considerably intense pink colours, with positive and considerably high a^* values (10.6–10.4; red hue) and small and positive b^* values (0.2–5.0; yellow hue). Thus, the increase in the Mg doping (x) results in a gradual evolution from purple to pink colours, which is accompanied by an increase of the red component (a^*), and a change from the blue (negative

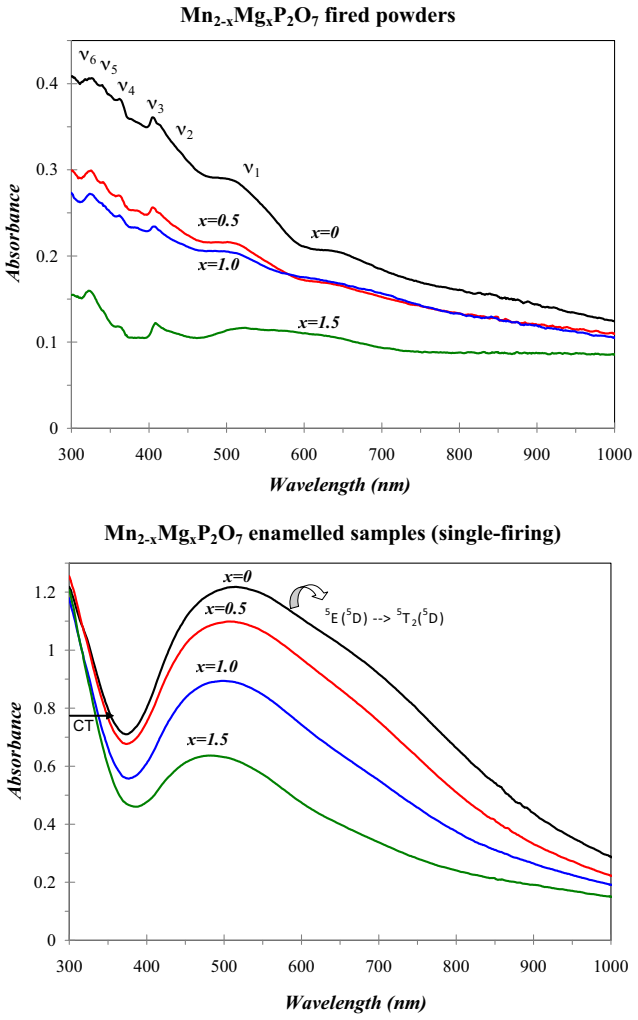

Fig. 6. Absorbance spectra corresponding to selected $Mn_{2-x}Mg_xP_2O_7$ diphosphate powders (above) and samples enamelled within the single-firing glaze (below).

b^*) to the yellow hue (positive a^*). Remarkably, the nice pinkish colours ($L^*/a^*/b^*$ values around 46–60/10.6–10.4/0.2–5.0) developed by Mg-enriched $Mn_{2-x}Mg_xP_2O_7$ solid solutions ($1.0 \leq x \leq 1.5$) are quite similar to those obtained with other conventional pink ceramic pigments, such as Mn–Al_2O_3 and Cr–Al_2O_3 corundum-based pigments (DCMA[41] numbers 3-04-5 and 3-03-5, respectively) or the $Zn(Al,Cr)_2O_4$ spinel-based pigment (DCMA number 13-32-5).[42,43] We performed additional tests enamelling the diphosphate powders (5 wt.%) with another transparent glaze having a different composition (SiO_2–Al_2O_3–B_2O_3–CaO–Na_2O–K_2O system), typical of a low-temperature double-firing schedule (melting around 1000 °C). Interestingly, similar purple ($x < 1$) and pink colourations ($1.0 \leq x \leq 1.5$) were obtained (the $L^*/a^*/b^*$ values of the pink colours were around 53–69/9.6–10.4/−1.3–3.0). Therefore, these thortveitite-based diphosphate solid solutions could be used as alternative pink ceramic dyes for the colouration of conventional (transparent) ceramic glazes melting at relatively low temperatures (below 1100 °C). It must be highlighted that they cannot be considered as ceramic pigments since they are not chemically inert within the glassy matrix (see Section 3.5). Further tests should be performed to confirm if these compounds can develop the same pinkish colourations when using ceramic glazes of higher firing temperatures (i.e. porcelainized Gres).

3.5. Interaction of fired diphosphates with the single-firing ceramic glaze

As it has been discussed in the previous section, the UV–vis characterization of enamelled samples demonstrated that a considerable amount of Mn^{2+} ions was oxidized to Mn^{3+} in the single-firing ceramic glaze during enamel firing. Accordingly, some interaction or reaction between the diphosphate powders and the ceramic glaze must occur during enamel firing. This effect was corroborated by performing SEM-EDX analyses onto the glassy surface of enamelled samples. As a complementary characterization, the particle size distribution of selected fired powders was previously measured (see Supplementary data in Appendix A). This characterization showed some appreciable differences in the particle size distribution of the powders, with a gradual decrease of the particle size with the increase of Mg doping (i.e., the values of the d_{50} diameter were 13.8, 8.2 and 5.2 μm for compositions with $x = 0$, 1.0 and 1.5, respectively; see Table A.1 and Figure A.1 in the appendix). This information is relevant, since the fired powders having a finer particle size (in this case, Mg-enriched samples) could interact or dissolve more easily in the molten glaze during enamel firing, and this could therefore affect to the colour developed by enamelled samples.

Nevertheless, the SEM/EDX analyses performed on enamelled samples confirmed quite a similar interaction of the diphosphate particles with the ceramic glaze in all samples. Irrespective of the different particle size distributions (and Mg content), most of the P and Mn of the diphosphate powders was leached or solubilized into the glassy matrix. As an example, Fig. 8a shows the SEM image of enamelled sample M1 ($x = 0$; $Mn_2P_2O_7$) obtained with the backscattered detector. In spite of the coarser particle size of M1 powders (according to the particle size characterization), this image confirms the extensive

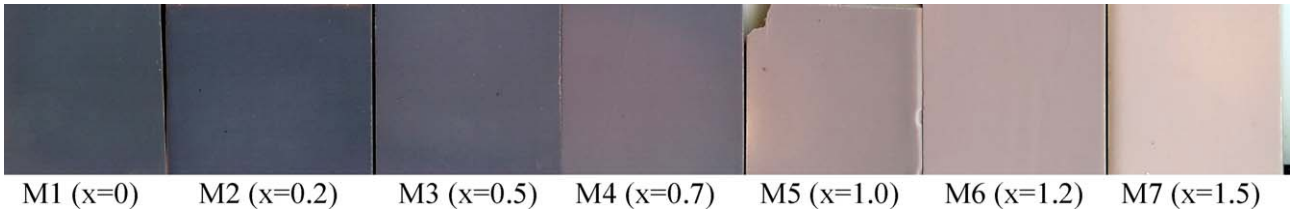

Fig. 7. Aspect of $Mn_{2-x}Mg_xP_2O_7$ diphosphate samples enamelled (5 wt.%) within a conventional single-firing ceramic glaze. (For appreciating the colour differences in this figure, the reader is referred to the web version of the article.)

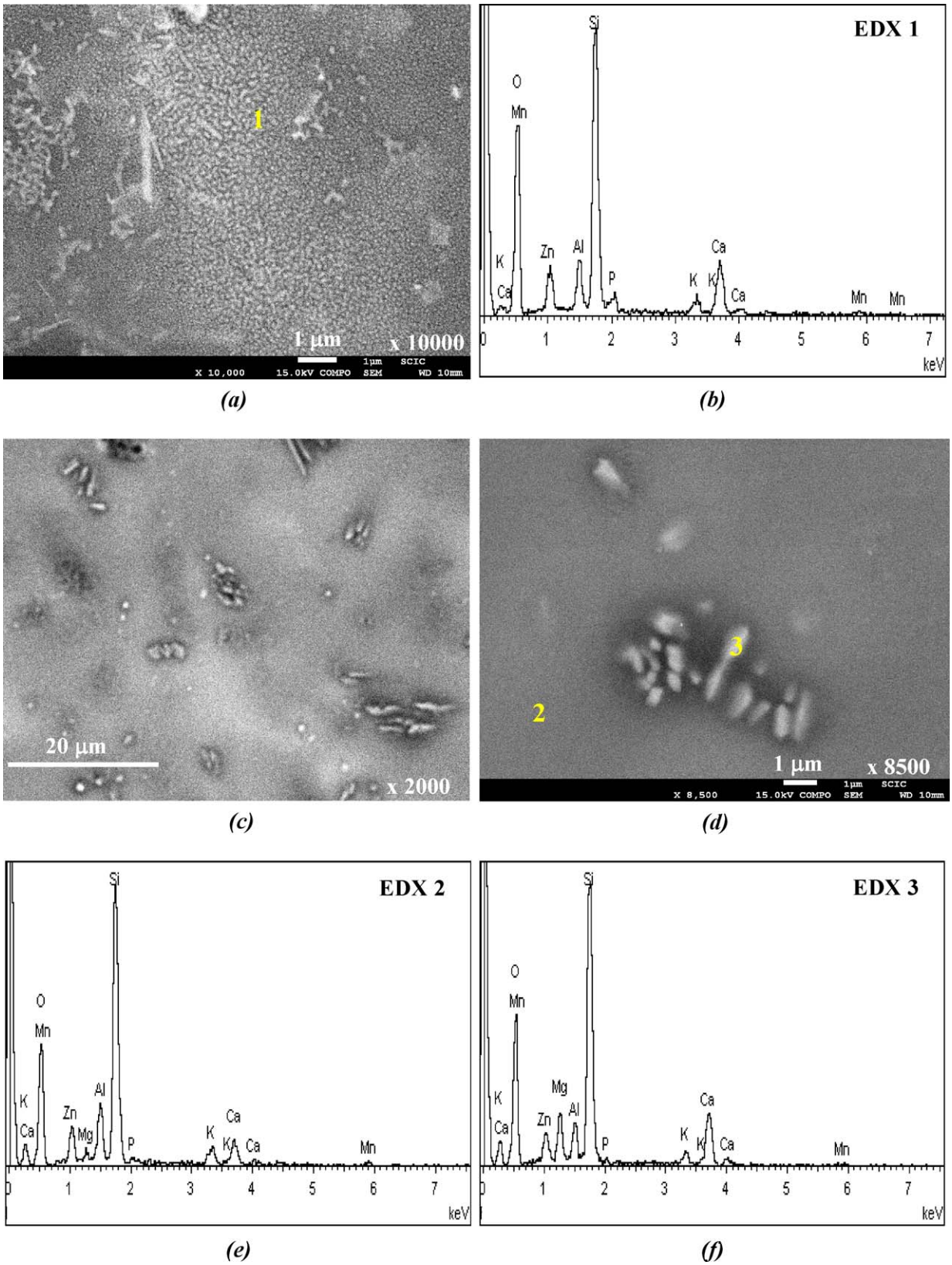

Fig. 8. SEM images (a, c and d) and EDX spectra (b, e and f) of samples enamelled (5 wt.%) within the single-firing glaze: (a and b) sample M1 ($x = 0$; $Mn_2P_2O_7$), and (c–f) sample M5 ($x = 1.0$; $Mn_{1.0}Mg_{1.0}P_2O_7$). The EDX spectra correspond to the local regions labelled as 1–3.

reaction of the diphosphate with the glaze, showing regions with very small (nanosized or submicronic) and brighter spots corresponding to pristine diphosphate particles partially solubilized or incorporated into the glassy matrix (see for instance in the region labelled as 1). The associated EDX spot-analysis of this region (shown in Fig. 8b) confirms the presence of some amount of P and Mn, along with other elements present in the glaze (Si, Al, Zn, Ca and K). Noteworthy, the EDX analyses indicate a higher signal of Ca in all these brighter regions associated to the decomposition of diphosphate powders, suggesting a high affinity of Ca ions to segregate from the glaze and interact with the diphosphate powders.

Similarly, Fig. 8c and d shows two representative SEM details of an Mg-enriched enamelled sample (M5, $x = 1.0$) at different magnifications, in which the presence of some particles dispersed in the glassy matrix may be also appreciated. The brighter regions would be indicating the presence of a higher amount of heavier elements (in this case, Zn, Mn, Ca and K). Noteworthy, the EDX spot analyses performed in the glassy regions (see for instance the EDX in Fig. 8e, corresponding to the region labelled as 2 in Fig. 8d) show the presence of P and Mn signals. The slightly weaker intensity of the P and Mn signals (with respect to M1 sample) is in agreement with the lower Mn content in this composition (M5), and it could be also indicating a more advanced (extensive) and homogeneous diffusion, or a faster solubilization of both elements into the glassy phase. On the other hand, the EDX spot-analyses performed onto the dispersed particles (i.e. see EDX of region 3 in Fig. 8f) indicate the presence of small amounts of Mn and P, and much higher amounts of Mg and Ca. Accordingly, the dispersed particles would correspond to the pristine Mn–Mg binary diphosphates partially decomposed by the reaction with the molten glaze. Thus, the chemical interaction between the dispersed diphosphate particles and the molten glaze during enamel firing is clearly evidenced by the segregation of calcium from the glaze to concentrate onto the diphosphate particles (irrespective of the Mg doping), and by the extensive leaching or solubilization of P and Mn species (mainly oxidized as Mn^{3+} ions, according to UV–vis spectra), that are more easily incorporated into the glassy matrix than Mg ions.

In summary, these analyses confirm that the diphosphate solid solutions would be acting as ceramic dyes, due to its reactivity (low stability) within the ceramic glaze, and the colouration mechanism would be mainly attributed to ion-colouring, given the extensive incorporation of Mn species (Mn^{3+}) into the glaze. Thus, the observed differences in the colouring performance ($L^*a^*b^*$ parameters) of enamelled samples would be mainly caused by the different concentrations of chromophore ions (Mn^{3+}) solubilized in the glaze.[37] Indeed, the obtained gradual variation of the colour from dark purple (low Mg doping) to light pink (high Mg doping) would be in agreement with the gradual decrease of the Mn content in the binary diphosphates and, accordingly, in the ceramic glaze.

4. Conclusions

In this study we prepared by the coprecipitation route and characterized for the first time a solid solution series of Mn and Mg mixed diphosphates ($Mn_{2-x}Mg_xP_2O_7$) within an extended compositional range ($x = 0.2$–1.5). XRD and SEM characterization confirmed the formation of isostructural and homogeneous β-$Mn_{2-x}Mg_xP_2O_7$ solid solutions having the thortveitite structure (monoclinic *C2/m* spatial group) within the whole range of studied compositions. A progressive decrease in the measured unit cell parameters was observed in accordance with the replacement of Mn^{2+} by the smaller Mg^{2+} ions. The fired diphosphate powders (1000 °C/4 h) exhibited light brown ($x < 1.0$) or pinkish-white ($1.0 \leq x \leq 1.5$) pale colours, owing to the low intensity optical absorption (300–650 nm) associated to the spin-forbidden transitions of Mn^{2+} ions in the distorted octahedral sites of thortveitite structure. Interestingly, the diphosphate samples developed intense purple ($x < 1.0$) or pinkish ($1.0 \leq x \leq 1.5$) colours once enamelled (5 wt.%) within a conventional single-firing ceramic glaze (enamel firing at 1080 °C). According to UV–vis-NIR characterization, these colours were mainly associated to the broad and complex absorption (400–800 nm) of Mn^{3+} ions in an octahedral environment. SEM-EDX analyses performed onto enamelled samples confirmed the chemical interaction of the diphosphate powders with the ceramic glaze, with an extensive solubilization of Mn (Mn^{3+}) and phosphate species into the glassy phase. The developed pink colours were similar to those obtained with other classical pink ceramic pigments and, accordingly, the thortveitite-based $Mn_{2-x}Mg_xP_2O_7$ diphosphate solid solutions ($1.0 \leq x \leq 1.5$) could be used as alternative pink ceramic dyes for the colouration of conventional ceramic glazes melting at relatively low temperatures (below 1100 °C).

Acknowledgements

The authors thank the Spanish "*Ministerio de Ciencia e Innovación*" (Project MAT2008-02893) and Universitat Jaume I (Project P1.1B2010-09) for financial support. Moreover, the technical assistance provided by the Central Services of Scientific Instrumentation (SCIC) of the University Jaume I, and by the Institute of Ceramic Technology (ITC) of Castellón is also fully acknowledged.

Appendix A. Supplementary data

Supplementary data associated with this article can be found, in the online version, at doi:10.1016/j.jeurceramsoc.2011.10.051.

References

1. Clark GM. Inorganic pyrocompounds $M_a[(X_2O_7)_b]$. *Chem Soc Rev* 1976;**5**:269–95.
2. Brown ID, Calvo C. The crystal chemistry of large cation dichromates, pyrophosphates, and related compounds with stoichiometry $X_2Y_2O_7$. *J Solid State Chem* 1970;**1**:173–9.
3. Boukhari A. Diphosphate structures related to the dichromate or thortveitite type. *J Alloys Compd* 1992;**188**:14–20.
4. Durif A. *Crystal chemistry of condensed phosphates*. 1st ed. New York: Plenum Press; 1995.

5. Parada C, Perles J, Sáez-Puche R, Ruiz-Valero C, Snejko N. Crystal growth, structure, and magnetic properties of a new polymorph of $Fe_2P_2O_7$. *Chem Mater* 2003;**15**:3347–51.
6. Calvo C. Refinement of the crystal structure of β-$Mg_2P_2O_7$. *Can J Chem* 1965;**43**:1139–46.
7. Stefanidis T, Nord AG. Structural studies of thortveitite-like dimanganese diphosphate, $Mn_2P_2O_7$. *Acta Cryst* 1984;**C40**:1995–9.
8. Robertson BE, Calvo C. Crystal structure of β-$Cu_2P_2O_7$. *Can J Chem* 1968;**46**:605–12.
9. Calvo C. The crystal structure and phase transitions of β-$Zn_2P_2O_7$. *Can J Chem* 1965;**43**:1147–53.
10. Boonchom B, Vittayakorn N. Synthesis and ferromagnetic property of new binary copper iron pyrophosphate $CuFeP_2O_7$. *Mater Lett* 2010;**64**: 275–7.
11. Baran EJ, Nord AG, Diemann E, Ericsson T. Electronic spectra of $(Mg,Co)_2P_2O_7$ phases. *Acta Chem Scand* 1990;**44**:513–5.
12. Ericsson T, Nord AG. Solid solutions of the type $(Ni,M)_2P_2O_7$. *Acta Chem Scand* 1990;**44**:990–3.
13. Maass K, Glaum R, Gruehn R. Contributions on crystal chemistry and thermal behaviour of anhydrous phosphates XXXI. $(Mg_{1-x}Cr_x)P_2O_7$, $CaCrP_2O_7$, $SrCrP_2O_7$ and $BaCrP_2O_7$—new diphosphates of divalent chromium. *Z Anorg Allg Chem* 2001;**627**:2081–90.
14. Boukhari A, Moqine A, Flandrois S. Synthesis and characterization of new copper (II) mixed diphosphates $(M,Cu)_2P_2O_7$ with M = Mg, Ca, Sr and Ba. *J Solid State Chem* 1990;**87**:251–6.
15. El-Bali B, Boukhari A, Aride J, Maass K, Wald D, Glaum R, et al. Crystal structure and colour of $SrNiP_2O_7$ and $SrNi_3(P_2O_7)_2$. *Solid State Sci* 2001;**3**:669–76.
16. Boonchom B, Danvirutai C. Synthesis of $MnNiP_2O_7$ and nonisothermal decomposition kinetics of a new binary $Mn_{0.5}Ni_{0.5}HPO_4{\cdot}H_2O$ precursor obtained from a rapid coprecipitation at ambient temperature. *Ind Eng Chem Res* 2008;**47**:5976–81.
17. Boonchom B, Phuvongpha N. Synthesis of new cobalt iron pyrophosphate $CoFeP_2O_7$. *Mater Lett* 2009;**63**:1709–11.
18. Onoda H, Yokouchi K, Kojima K, Nariai H. Addition of rare Earth cation on formation and properties of various cobalt phosphates. *Mater Sci Eng B* 2005;**116**:189–95.
19. Onoda H, Matsui H, Tanaka I. Improvement of acid and base resistance of nickel phosphate pigment by the addition of lanthanum cation. *Mater Sci Eng B* 2007;**141**:28–33.
20. Onoda H, Kojima K, Nariai H. Additional effects of rare earth elements on formation and properties of some transition metal pyrophosphates. *J Alloys Compd* 2006;**408**(412):568–72.
21. Meseguer S, Tena MA, Gargori C, Badenes JA, Llusar M, Monrós G. Structure and colour of cobalt ceramic pigments from phosphates. *Ceram Int* 2007;**33**:843–9.
22. Meseguer S, Tena MA, Gargori C, Badenes JA, Llusar M, Monrós G. Development of blue ceramic dyes from cobalt phosphates. *Ceram Int* 2008;**34**:1431–8.
23. Llusar M, Badenes JA, García A, Gargori C, Galindo R, Monrós G. Solid solutions of mixed metal $Mn_{3-x}Mg_xFe_4(PO_4)_6$ orthophosphates: colouring performance within a double-firing ceramic glaze. *Ceram Int* 2011;**37**:493–504.
24. Llusar M, Zielinska A, Tena MA, Badenes JA, Monrós G. Blue-violet ceramic pigments based on Co and $Mg{\cdot}Co_{2-x}Mg_xP_2O_7$ diphosphates. *J Eur Ceram Soc* 2010;**30**:1887–96.
25. Boonchom B. Kinetic and thermodynamic studies of $MgHPO_4{\cdot}3H_2O$ by non-isothermal decomposition data. *J Therm Anal Calorim* 2009;**98**:863–71.
26. Maass K. New studies about quaternary phosphates of divalent 3d-transition metals. Ph.D. thesis, Justus-Liebig University, Giessen, Germany; 2002 [translated from the German version].
27. Bruker AXS. *TOPAS V2.1. General profile and structure analysis software for powder diffraction data. User's manual, Bruker AXS*. Bruker AXS: Karlsruhe, Germany; 2003.
28. Cheary RW, Coelho AA. A fundamental parameters approach to X-ray line-profile fitting. *J Appl Crystallogr* 1992;**25**:109–21.
29. CIE. *Recommendations on uniform colour spaces, colour difference equations, psychometrics colour terms. In Supplement No. 2 of CIE Publ. No.15 (E1-1.31) 1971*. Paris: Bureau Central de la CIE; 1978.
30. Danvirutai C, Noisong P, Youngme S. Some thermodynamic functions and kinetics of thermal decomposition of $NH_4MnPO_4{\cdot}H_2O$ in nitrogen atmosphere. *J Therm Anal Calorim* 2010;**100**:117–24.
31. Kongshaug KO, Fjellvåg H, Lillerud KP. Synthesis and ab-initio structure determination of organically templated magnesium phosphates from powder diffraction data. *J Mater Chem* 2000;**10**:1915–20.
32. Wu J, Yuan AQ, Huang ZY, Tong ZF, Chen J, Liang RL. Thermochemical properties and decomposition kinetics of ammonium magnesium phosphate monohydrate. *Chin J Chem* 2007;**25**:72–6.
33. ICSC. *Inorganic crystal structure database, developed by FIZ Karlsruhe*; 2009. The new ICSD Web is available from June 2009 at http://icsd.fiz-karlsruhe.de/icsd.
34. Shannon RD. Revised effective ionic radii and systematic studies of interatomic distances in halides and chalcogenides. *Acta Crystallogr* 1976;**A32**:751–67.
35. Duffy JA. *Bonding energy levels & bands in inorganic solids*. United Kingdom: Longman Group UK Limited; 1990.
36. Glaum R, Thauern H, Schmidt A, Gerk M. Contributions on the bonding behaviour of oxygen in inorganic solids III. $Mn_2P_4O_{12}$, $Mn_2Si(P_2O_7)_2$ and $Mn_2P_2O_7$—crystal growth, structure refinements and electronic spectra of manganese(II) phosphates. *Z Anorg Allg Chem* 2002;**628**:2800–8.
37. Konikadis I, Varsamis CPE, Kamitsos EI, Möncke D, Ehrt D. Structure and properties of mixed strontium–manganese metaphosphate glasses. *J Phys Chem C* 2010;**114**:9125–38 [and references 48–54 therein].
38. Singh SP, Kumar A. Absorption spectrum of Mn^{3+} and redox equilibria of iron and manganese in sodium silicate glass. *Phys Chem Glasses* 1992;**33**:61–7.
39. Kawano M, Takebe H, Kuwabara M. Compositional dependence of the luminescence properties of Mn^{2+}-doped methaphosphates glasses. *Opt Mater* 2009;**32**:277–80.
40. Machado IEC, Prado L, Gomes L, Prison JM, Martinelli JR. Optical properties of manganese in barium phosphate glasses. *J Non-Cryst Solids* 2004;**348**:113–7.
41. DCMA. *Classification and chemical description of the mixed metal oxide inorganic coloured pigments*. 2nd ed. Washington, DC: Dry Color Manufacturer Association; 1982.
42. López-Navarrete E, Ocaña M. Aerosol-derived Mn-doped Al_2O_3 pink pigments prepared in the absence of fluxes. *Dyes Pigments* 2004;**61**:279–86.
43. Martos M, Martínez M, Cordoncillo E, Escribano P. Towards more ecological ceramic pigments: study of the influence of glass composition on the colour stability of a pink chromium-doped ceramic pigment. *J Eur Ceram Soc* 2007;**27**:4561–7.